



Hybridization and Power Control of an Isolated PV-SEIG-based Generation System Using novel Nine Switch Converter

Abhijeet Choudhury¹, Swagat Pati¹, Sanjeeb Kumar Kar¹, Renu Sharma²

¹Department of Electrical Engineering, ITER, Siksha O Anusandhan Deemed to be University, Bhubaneswar, Odisha, India.

²Department of Electrical Engineering, Siksha O Anusandhan Deemed to be University, Bhubaneswar, Odisha, India.

Cite this article as: A. Choudhury, S. Pati, S. Kumar Kar and R. Sharma, "Hybridization and power control of an isolated PV-SEIG-based generation system using novel nine switch converter," *Electrica*, 23(1), 28-39, 2023.

ABSTRACT

This study introduces a novel nine switch converter topology for integration and power flow between hybrid Self-excited induction generator - Photovoltaic (SEIG-PV)-based isolated system. The hybrid isolated system houses a 22-kW SEIG, an 18-kW photovoltaic system, and Battery Energy Storage System (BESS). Nine switch converter plays a vital role by providing continuous power supply irrespective of load or source side disturbances and helps in managing the power flow throughout the system. Two separate decoupled control strategies have been designed for source side and load side, which helps in regulating the voltage and frequency to be constant for both ends. The self-excited induction generator side power control strategy regulates the power flow and changes the DC-link voltage such that the excess/deficit power is stored/extracted from BESS. The whole system is subjected to two different loads, that is, linear load and dynamic load, and the uninterruptible power flow capability is also analyzed. The entire system has been simulated and modeled using Matrix Laboratory (MATLAB)-2018(a).

Index Terms—Battery energy storage system, decoupled control, nine switch converter, photovoltaic system, self-excited induction generator, uninterrupted power supply

Corresponding author:

Abhijeet Choudhury

E-mail:

abhijeet9966@gmail.com

Received: September 27, 2021

Revised: March 25, 2022

Accepted: May 8, 2022

Publication Date: July 27, 2022

DOI: 10.5152/electrica.2022.21120



Content of this journal is licensed under a Creative Commons Attribution-NonCommercial 4.0 International License.

I. INTRODUCTION

Electrical power generation so far has included thermal, nuclear, and hydropower plants. This has almost led to continuous degradation of environmental conditions. Depletion of conventional energy sources has been increasing at a faster rate for which renewable energy sources are now been brought into the picture. Renewable energy sources have a number of variants such as micro-hydro, wind, PV, fuel cell, etc. Among these, the authors have considered the micro-hydro and photovoltaic system, hybridized both with a BESS focused on the power flow control in the system. Taking into consideration the micro-hydro-based SEIG system, it has been seen that the control of " f " and " V " of SEIG has been most challenging. Though SEIGs inherit characteristics including robustness, maintenance-free, and economically viable, but yet these machines show stability issues which have been often investigated by authors in case of isolated system operation. Moreover, it has been noticed that the voltage and frequency of the system vary when fluctuations are observed in loads " P " or " Q " power demand. Excitation capacitance requirement for SEIG-based system given in [1] greatly depends on the reactive power requirement of the generator, for flux generation, and the reactive power supply capacity of the system. Failure in excitation and severe voltage dips, as well as total blackout, have been observed in the case of SEIG-based isolated systems when there is sudden reactive power demand. To regulate the voltage of SEIG, a lot of research has been done. A fair amount of voltage regulation can be achieved by using a combination of series and shunt capacitances that are delineated in [2,3]. In literature, the use of saturable core reactors as stated in [4], Static Var Compensator (SVC) detailed description in [5], and the converter-based series and shunt compensators [6,7] have also been investigated for regulating the voltage in the SEIG system. Among different strategies for voltage control of SEIG, most effectiveness and efficiency have been observed in the case of Static Synchronous Compensator (STATCOM) as given in [7,8].

In order to maintain the frequency support of a SEIG-based isolated system, a combination of STATCOM and BESS has been delineated in [9-15]. Although electronic load controller helps in mitigating the frequency demand in SEIG systems [10], electronic load controllers more often

dissipate a lump sum amount of power at dump load which moreover leads to inefficiency of the system. Finding a solution to this issue, many researchers have opted for the hybridization of energy sources. [11] provides information about a SCIG-based wind energy conversion system hybridized with micro-hydro system housing SEIG using back to back converters, which helps in easy integration of energy source and controls the power flow. Literature [11,16,17] depicts that the loads are directly connected to the terminals of SEIG. This layout causes serious drawbacks, that is, when the load fluctuates, disturbances are observed in the SEIGs current which leads to variation in voltage and frequency of the SEIG. Again, this type of arrangements of SEIG leads to a complete shutdown of the system even in the presence of BESS, during any fault in SEIG.

Looking into the scenario, nine switch converter (NSC) can be chosen as an effective solution for all the above-mentioned problems. Two independent loads operating at different frequencies and voltages can be supplied from a single NSC. This extraordinary feature of NSC is quite capable of integrating different renewable energy sources. In comparison with back to back converter, NSC is quite economical as it poses nine bidirectional switches. Decoupled power control is possible in the case of NSC because of the presence of a DC-link. Therefore, two different control algorithms can be imparted in order to control both load and SEIG separately, which would help in stabilizing the voltage and frequency of SEIG irrespective of rigorous load fluctuation. Again, there exists another possibility of continuous supply to the load, irrespective of disturbance on source side, which has also been investigated in this work.

In this study, a hybrid isolated system is taken into consideration. The hybrid system is formed by the integration of SEIG, PV, BESS, and load through an NSC. The two major aspects which are considered in this study are power control in the system using NSC and the capability of the system to provide continuous power supply during source

side disturbances and source disconnection. For power control of the source and the load side of NSC, two different control strategies have been discussed in this work. The SEIG side power flow is controlled by a decoupled current component-based control strategy. This control structure regulates the voltage and frequency of the SEIG by appropriate management of the active and reactive power. The load side control structure regulates the load side voltage and frequency, irrespective of load and source disturbances. The performance of the NSC for power control is examined and analyzed by switching two different loads into the system, that is conventional RL load and induction motor load. The hybrid system is also examined under source side disturbances likely step variation in prime mover torque of the SEIG and source disconnection. MATLAB and Simulink environment is used for modeling and simulation of the work presented in this study.

II. SYSTEM CONFIGURATION

A hybrid isolated system is taken into consideration which comprises SEIG, PV, and energy storage system, all of which are integrated through a power converter. The architectural representation is shown in Fig. 1.

In [7-11], it can be noticed that the loads are directly connected to the SEIG system. In this study, the proposed configuration is dynamic, reliable, and efficient as compared to the literature. Here, in this proposed configuration, an independent power control strategy has been used both for the generation side and load side. So, any fluctuation in the load end does not affect the generation side voltage and frequency. Similarly, supply to the load is possible if any one source, that is, either PV or SEIG is disconnected. Nine switch converter enhances the cost-effectiveness of the system with switch count minimization as compared to conventional six switch back to back (B2B) converters. Moreover, in the case of NSC, the gate pulse for middle set is obtained from the XOR operation of top and bottom sets of switches. For this reason, no extra dead time has to be introduced in the gate pulses of

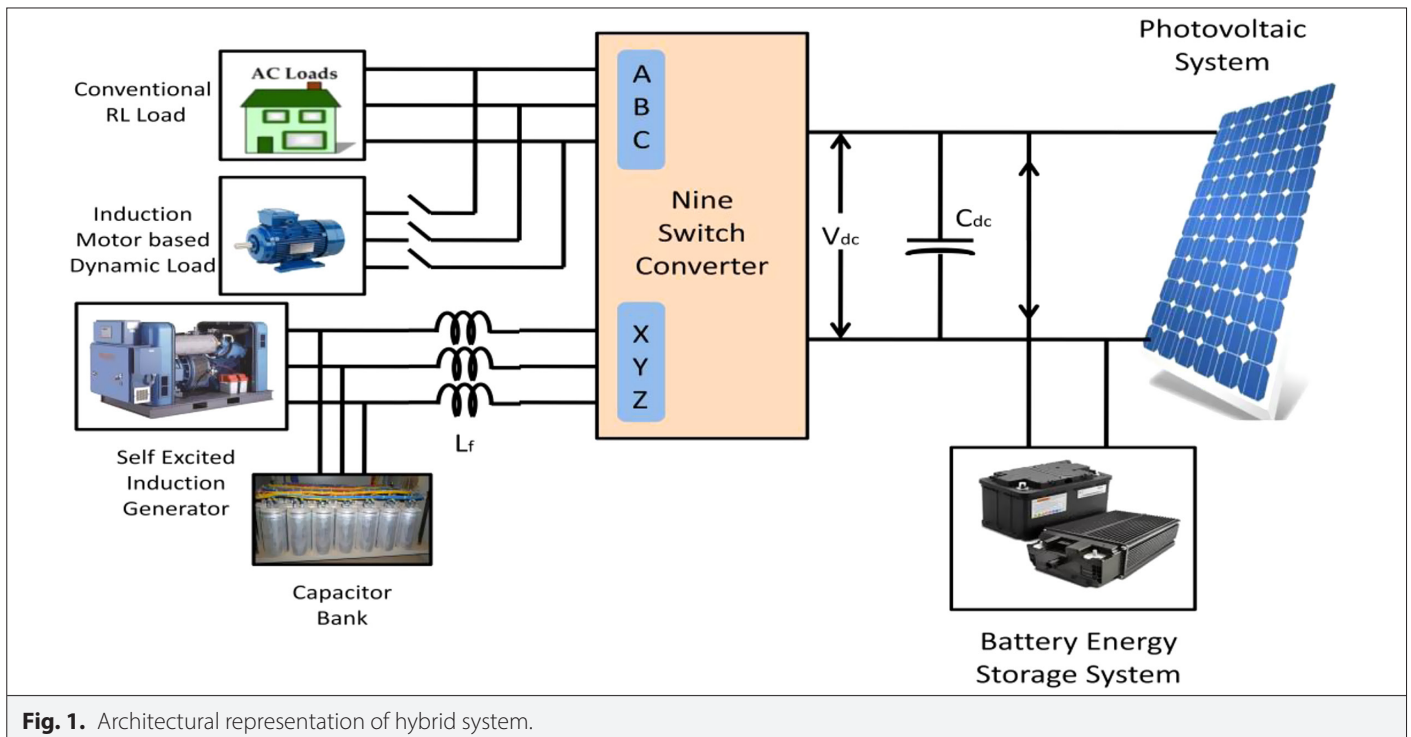


Fig. 1. Architectural representation of hybrid system.

each phase leg which significantly increases the reliability of the NSC. One of the major cons is possessed by NSC, that is increased DC-link voltage requirement as compared to back to back converters.

III. NSC STRUCTURES AND CONTROL STRATEGIES

A. Nine Switch Converter

The architectural representation of NSC is given in Fig. 2. The name of the converter itself suggests that it houses nine bi-directional switches. Furthermore, DC-link helps in controlling the two AC outputs/inputs independently as given in [18-20]. For this extraordinary feature of separate control of two AC sides of the NSC, it is suitable for hybrid isolated systems. The NSC is divided into three switch sets, namely, top set (T_i), middle set (M_i), and bottom set (B_i) where "i" denotes the phase leg number, that is, 1, 2, 3. It consists of two, 3-phase AC outputs. Here, in the present configuration, a three-phase self-excited induction generator is controlled through its XYZ terminal, and the load for the proposed system is connected to the terminals ABC as given in Fig. 2.

The necessary condition will be that in any phase leg, only two switches can remain ON at any point of time. Therefore, the necessary generalized form to enhance the logic of switching sequence is stated in (1).

$$T_i + M_i + B_i = 2 \quad (1)$$

This implies that three different switching combinations for any one phase legs are possible. The switching combinations with three switching states and the respective voltages at both outputs w.r.t DC midpoint are shown in Table I.

Apart from (1), the switching state of each phase leg can be equated as

$$T_i + M_i B_i = 1 \quad (2)$$

$$B_i + M_i T_i = 1$$

$$V_{p0} = (T_i - M_i B_i) \frac{V_d}{2} \quad (3)$$

$$V_{q0} = (T_i M_i - B_i) \frac{V_d}{2}$$

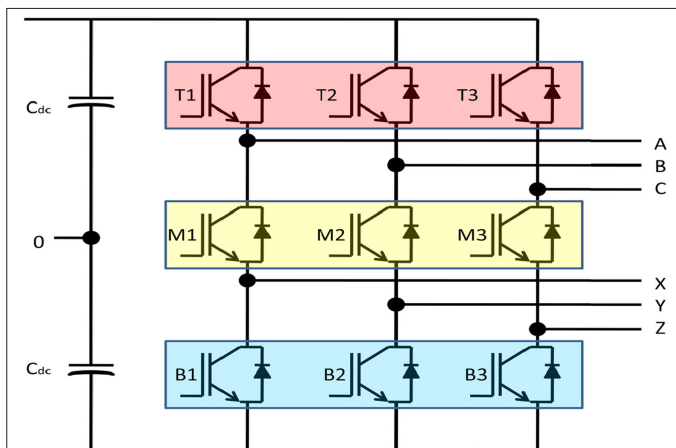


Fig. 2. Architectural representation of NSC. NSC, nine switch converter.

TABLE I. VOLTAGES WITH RESPECT TO DC MIDPOINT

T_i	M_i	B_i	V_{Ao}	V_{Xo}
1	1	0	$\frac{V_d}{2}$	$\frac{V_d}{2}$
1	0	1	$\frac{V_d}{2}$	$-\frac{V_d}{2}$
0	1	1	$-\frac{V_d}{2}$	$-\frac{V_d}{2}$
T_2	M_2	B_2	V_{Bo}	V_{Yo}
1	1	0	$\frac{V_d}{2}$	$\frac{V_d}{2}$
1	0	1	$\frac{V_d}{2}$	$-\frac{V_d}{2}$
0	1	1	$-\frac{V_d}{2}$	$-\frac{V_d}{2}$
T_3	M_3	B_3	V_{Co}	V_{Zo}
1	1	0	$\frac{V_d}{2}$	$\frac{V_d}{2}$
1	0	1	$\frac{V_d}{2}$	$-\frac{V_d}{2}$
0	1	1	$-\frac{V_d}{2}$	$-\frac{V_d}{2}$

where, p = phase A, B, C

q = phase X, Y, Z

$$i = \begin{cases} 1 & \text{for Phases A and X} \\ 2 & \text{for Phases B and Y} \\ 3 & \text{for Phases C and Z} \end{cases} \quad \text{Substituting (2) in (3), we get,}$$

$$V_{p0} = \{T_i - (1 - T_i)\} \frac{V_d}{2} = (2T_i - 1) \frac{V_d}{2} \quad (4)$$

$$V_{q0} = \{(1 - B_i) - B_i\} \frac{V_d}{2} = (1 - 2B_i) \frac{V_d}{2}$$

B. Control of SEIG system

The SEIG side control structure is designed to regulate the voltage and frequency of the SEIG. This control scheme basically manages the active and reactive power of the SEIG side. The proposed control structure is an orthogonal current component-based control scheme. In this scheme, the orthogonal components, that is, in-phase and quadrature components of the voltage, are used to control the frequency and voltage of the system. The in-phase component controls the system's active power, whereas the quadrature component is used for controlling the reactive power of the system. The active power management is done such that the excess/deficit power is stored in/drawn from the battery energy storage system which is connected to the DC-link of the NSC. The control scheme

also enables reactive power support for the SEIG side to maintain a constant voltage. The voltages from SEIG are sensed from its terminal, and the peak voltage is derived as:

$$V_T = \sqrt{\frac{2}{3}(V_A^2 + V_B^2 + V_C^2)} \quad (5)$$

The peak voltage " V_T " is then divided by the individual voltages to achieve the in-phase components as in (6).

$$u_A = \frac{V_A}{V_T}, u_B = \frac{V_B}{V_T}, u_C = \frac{V_C}{V_T} \quad (6)$$

After the in-phase components are found out, they are used to estimate the quadrature components. Equation (7) gives the calculation of w_A, w_B, w_C which are the quadrature components as given in [8].

$$\begin{bmatrix} w_A \\ w_B \\ w_C \end{bmatrix} = \begin{bmatrix} 0 & -\frac{1}{\sqrt{3}} & \frac{1}{\sqrt{3}} \\ \frac{\sqrt{3}}{2} & \frac{1}{2\sqrt{3}} & -\frac{1}{2\sqrt{3}} \\ -\frac{\sqrt{3}}{2} & \frac{1}{2\sqrt{3}} & -\frac{1}{2\sqrt{3}} \end{bmatrix} \begin{bmatrix} u_A \\ u_B \\ u_C \end{bmatrix} \quad (7)$$

Both the in-phase and quadrature components have unity amplitude and are displaced by 90° from each other.

In order to estimate the amplitudes of the in-phase and quadrature current components, the errors of voltage and frequency are sensed and fed to PI controllers:

$$I_{up}(n) = I_{up}(n-1) + K_{iu}e_{rrf}(n) + K_{pu}(e_{rrf}(n) - e_{rrf}(n-1)) \quad (8)$$

$$I_{wp}(n) = I_{wp}(n-1) + K_{iw}e_{rrv}(n) + K_{pw}(e_{rrv}(n) - e_{rrv}(n-1)) \quad (9)$$

where

$$e_{rrf} = f^* - f \quad (10)$$

$$e_{rrv} = V_{tref} - V_t \quad (11)$$

where " f " is the frequency, " f^* " is the reference frequency, " V_t " is the terminal voltage and " V_{tref} " is the reference terminal voltage. K_{pu} , K_{pw} , K_{iu} and K_{iw} are the proportional and integral gains of the PI controllers.

I_{up} and I_{wp} are the amplitudes of in-phase and quadrature current components, respectively. The in-phase and quadrature current components are calculated by multiplying their respective amplitudes with their unit vectors which are given by (12) and (13).

$$I_{ua} = I_{up} \times u_a \quad (12)$$

$$I_{ub} = I_{up} \times u_b$$

$$I_{uc} = I_{up} \times u_c$$

$$I_{wa} = I_{wp} \times w_a$$

$$I_{wb} = I_{wp} \times w_b \quad (13)$$

$$I_{wc} = I_{wp} \times w_c$$

After getting the in-phase and quadrature currents, the three-phase reference currents are calculated as in (14)

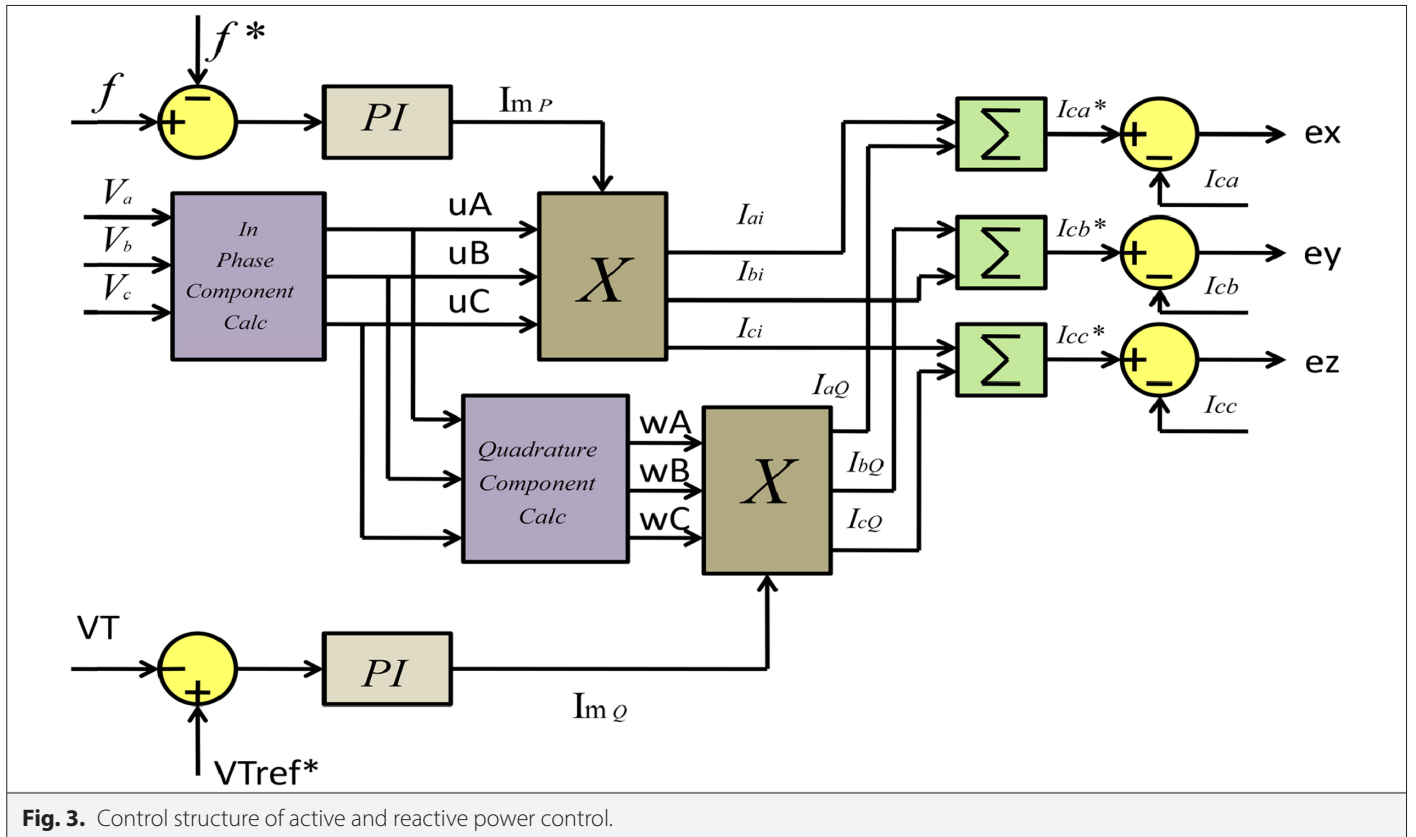


Fig. 3. Control structure of active and reactive power control.

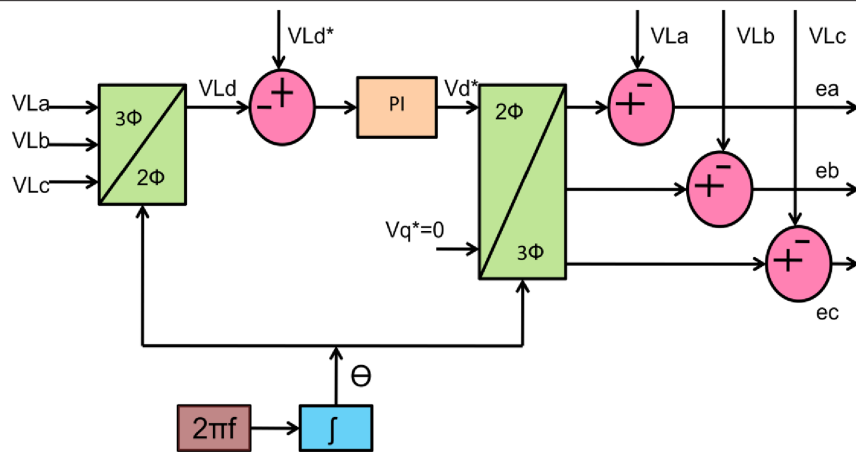


Fig. 4. Control structure of load side voltage control.

$$i_a^* = i_{ua} + i_{wa}$$

$$i_b^* = i_{ub} + i_{wb} \quad (14)$$

$$i_c^* = i_{uc} + i_{wc}$$

The control signals for terminal XYZ, that is, " e_x ", " e_y ", " e_z " are calculated by subtracting the actual current values from their reference quantities as in (15).

$$e_x = i_a^* - i_a$$

$$e_y = i_b^* - i_b \quad (15)$$

$$e_z = i_c^* - i_c$$

Fig. 3 shows the control architecture for the power control of the SEIG side.

C. Load Side Voltage Control

In this section, the main focus is to improve the load end power quality. In order to maintain a constant voltage and frequency at the load end, a robust control strategy has been developed which seems to be quite efficient. A decoupled voltage control strategy has been implemented to enhance the load end power quality. Fig. 4 shows the control architecture of the load side.

In this control strategy, authors have focused to align the whole load side voltage with the direct axis of the reference frame. This makes the quadrature axis component of the load voltage to be zero. This way the load side voltage can be controlled by controlling only the direct axis voltage component, which reduces the number of controlled in the structure and makes the structure simpler. To implement the control structure, the direct axis component of load voltage is sensed and compared with its reference value. The error is given to a PI controller which generates the direct axis control voltage. The quadrature axis control voltage is set to zero. The direct and quadrature axis control voltages are then transformed to three-phase reference voltages, and the reference voltages are then compared with the three-phase load voltages to generate the control signals for the load side, that is, " e_a, e_b, e_c ". These control signals are used for the carrier-based switching of the NSC.

D. Nine switch converter switching

Mostly two different modulation strategies have been mentioned in literature for the switching of NSC, that is, space vector modulation

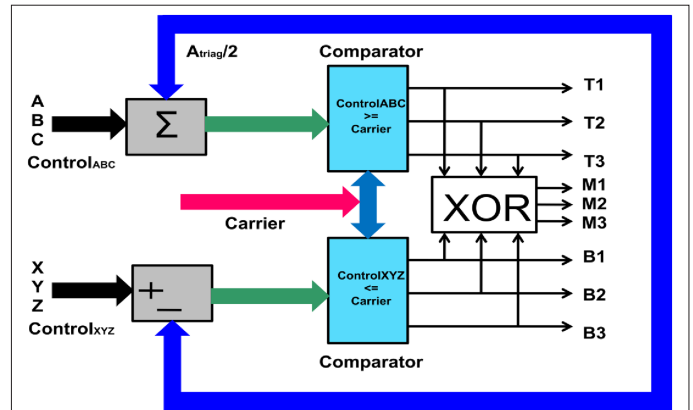


Fig. 5. Control structure of NSC switching. NSC, nine switch converter.

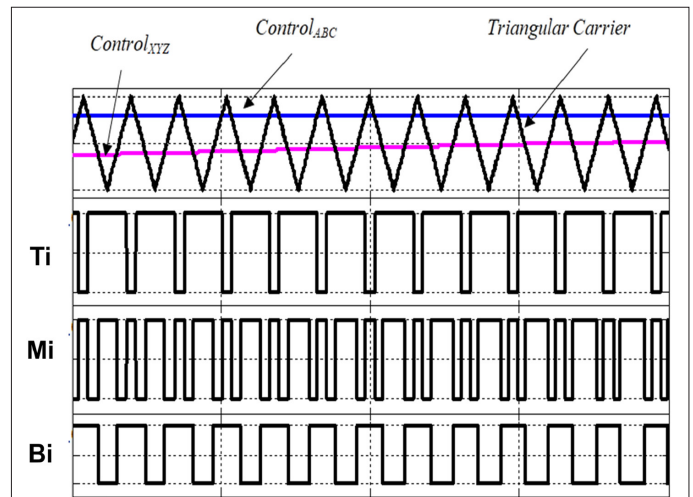


Fig. 6. Representation of reference switching signals of NSC. NSC, nine switch converter.

(SVM) [12] and carrier-based modulation [19]. In this work, carrier-based modulation technique is employed for the generation of gate pulse for NSC. The control signals " $e_{a_r}e_{b_r}e_{c_r}$ " and " $e_{x_r}e_{y_r}e_{z_r}$ " have been compared with a fixed frequency triangular carrier wave as given in Fig. 5.

For that to happen, the control signals " $e_{a_r}e_{b_r}e_{c_r}$ " and " $e_{x_r}e_{y_r}e_{z_r}$ " are given the required offset so that they do not intersect with each other. The offset given to the control signals also decides the effective aDC voltages which would be reflected at the terminals A, B, C and X, Y, Z. To achieve efficient switching of the NSC, it is to be taken care that the two sets of control signals " $e_{x_r}e_{y_r}e_{z_r}$ " and " $e_{a_r}e_{b_r}e_{c_r}$ " do not intersect with each other. The more the offset, the lesser will be the voltage. Hence, the offsets are adjusted according to the DC voltage requirement of terminals A, B, C and X, Y, Z. In this work, the total DC-link voltage is taken to be 1800 V. As both the generator and load sides are operated at 230 V phase voltage, both the sides have the same DC-link

voltage requirement. So, the DC voltage requirement for terminals "A, B, C" and "X, Y, Z" is taken to be equal. Hence, the offset given to the control signal in this work is equal. The offset taken in this work is " $\frac{V_{mTriag}}{2}$ " for control signals " $e_{a_r}e_{b_r}e_{c_r}$ " and " $e_{x_r}e_{y_r}e_{z_r}$ ". The reference switching signal is shown in Fig. 6.

The crucial arrangement in order to get the switching pulses for top set of switches can be obtained from:

$$T_i = \begin{cases} 1 & \text{if } Control_{ABC} > Carrier \\ 0 & \text{otherwise} \end{cases} \quad (16)$$

Likewise, for the bottom set of switches

$$B_i = \begin{cases} 1 & \text{if } Control_{XYZ} < Carrier \\ 0 & \text{otherwise} \end{cases} \quad (17)$$

The conditions for switching of middle set can be obtained by

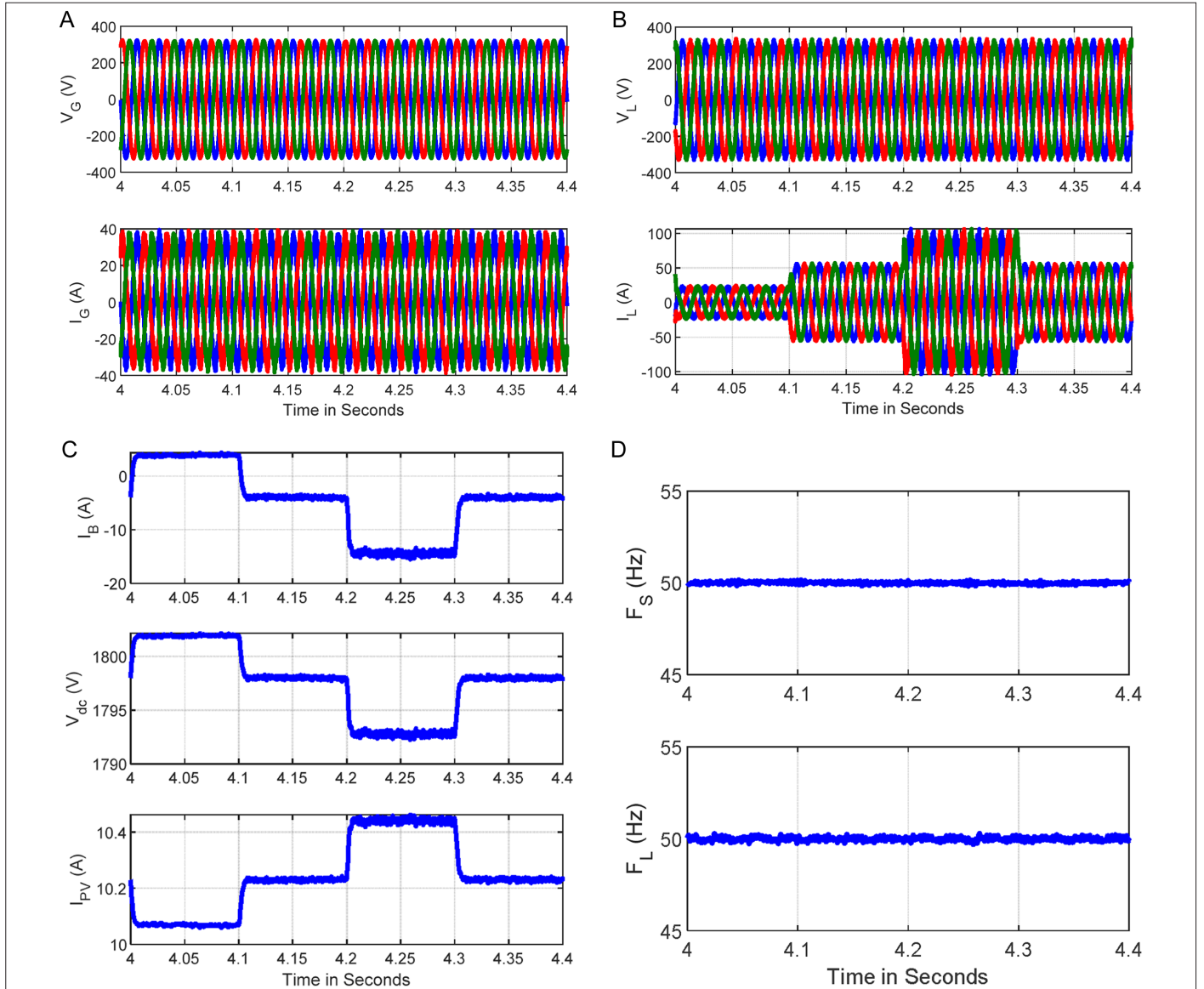


Fig. 7. (a) Voltage and current waveforms of source side. (b) Voltage and current waveforms of load side. (c) DC parameters waveforms of linear RL load. (d) Frequencies of both source and load side.

$$M_i = T_i \otimes B_i \quad (18)$$

The XOR (\otimes) operation ensures that in a phase leg, three switches cannot remain ON as given in [18-20]. This operation also helps in maintaining the required dead time between three switches in each phase leg, which is proficient and reliable as compared to B2B converters.

IV. SIMULATION RESULTS AND DISCUSSIONS

This work largely emphasizes on two objectives. The first objective is to regulate the voltage and frequency of the considered hybrid autonomous system using NSC, and second objective is to test the uninterrupted power supply capability of the system. The viability of the NSC for accomplishing the previously mentioned objective is assessed by exposing the system to various loads and source side disturbances. The response of the system is first assessed by oppressing the system to load side variations. Two different load variations are considered in this work. Namely,

- Conventional RL load;
- Induction motor-based dynamic load.

Then, the response of the system is evaluated for source side disturbances such as:

- Step variation in SEIG torque;
- Step change in illumination of PV.

And finally, the capability of the NSC for supplying uninterrupted power is evaluated by exposing the system to partial and total disconnection of the sources.

- *Performance Evaluation with Load Side Variation*

A. Simulation Analysis with Conventional RL Load

This segment depicts the system behavior while supplying an RL type load which is time-varying in nature. The source-side voltage and current waveforms stay undisturbed as can be seen in Fig. 7(a). The increment and reduction in current can be noticed in Fig. 7(b).

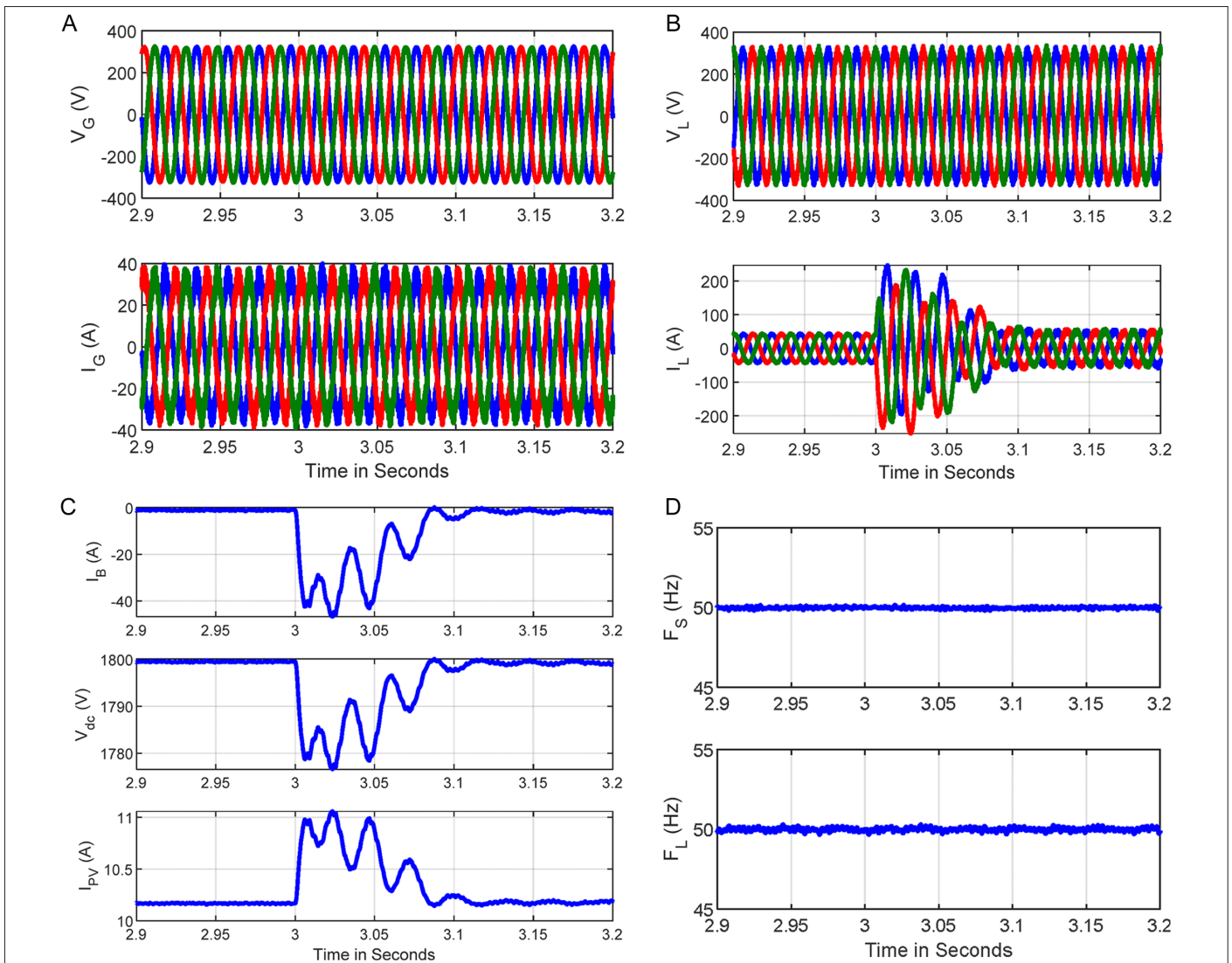


Fig. 8. (a) Voltage and current waveforms of source side. (b) Voltage and current waveforms of load side. (c) DC parameters waveforms of dynamic load switching. (d) Frequencies of both source and load Side.

The load end voltage is genuinely steady due to load side control structure as can be found in Fig. 7(b). Despite the variance in load, the frequency, current, and voltage of the SEIG are kept up at steady values. From Fig. 7(c), it is clear that there is an increase in DC-link when the load is less, for example from 4 seconds to 4.1 seconds. Due to the increase in DC-link voltage, the real power is diverted to the BESS which helps in making the frequency of the SEIG steady at 50 Hz as given in Fig. 7(d). During light loads, the PV current decreases

because of the increase in DC-link voltage, and the PV current rises during 4.2–4.3 seconds as a result of the fall in the DC-link voltage which is obvious from Fig.7 (c).

B. Simulation Analysis with Induction Motor-based Dynamic Load

In this part, the system performance is evaluated by switching a dynamic induction motor load to the system while the system is supplying power to a constant RL load previously. The induction motor

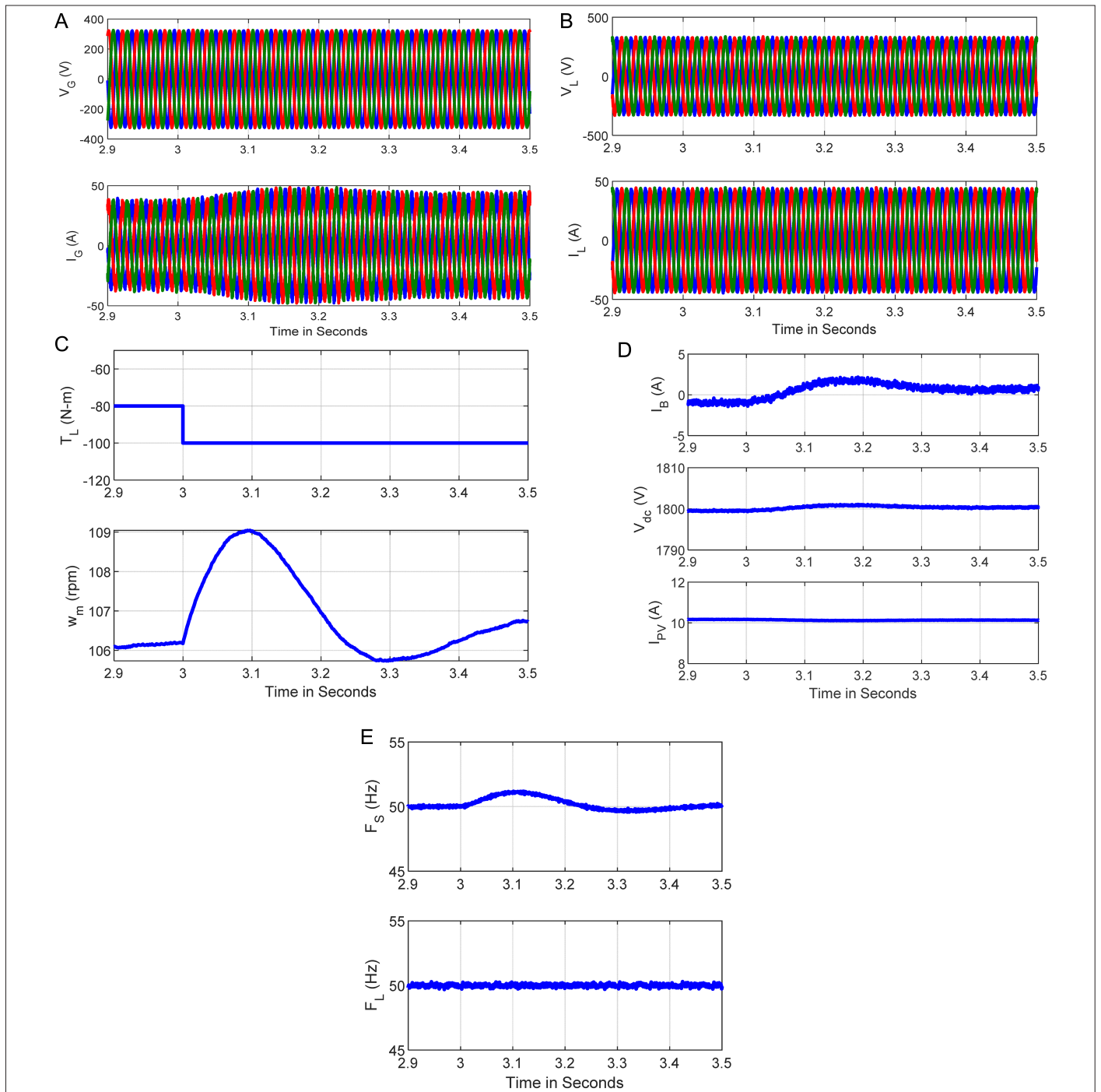


Fig. 9. (a) Source side voltage and current wave shapes during torque variation. (b) Load side voltage and current wave shapes during torque variation. (c) Torque and Speed wave shapes during torque variation. (d) DC parameters wave shapes during torque variation. (e) Frequencies of both Source and Load side during torque variation.

considered in the work is a 7.5 kW induction machine that is directly turned ON without any soft switching mechanism. A substantial disturbance in load current response is visible in Fig. 8(b) due to the sudden requirement of real and reactive power. There appear to be no changes on the source side as can be seen from Fig. 8(a) due to induction motor-based dynamic load switching. A voltage drop of around 20 V in the DC-link voltage occurs due to the sudden demand for real power. The drop in DC-link voltage forces the BESS to discharge and provide the required real power to the system. The rise in BESS current is visible in Fig. 8(c). The drop in DC-link voltage also results in the increase in the PV current which can be seen in Fig. 8(c). The load and SEIG side frequencies remain undisturbed in spite of severe load changes as given in Fig. 8(d), which demonstrates vigorous and productive power control done by the NSC.

• Performance Evaluation with Source Side Disturbance

C. Performance Analysis with Prime Mover Torque Variation at Source Side

In this section, a step change in the turbine torque is given at time 3 seconds. The turbine torque is increased from 80 Nm to 100 Nm as given in Fig. 9(c), due to which the power generated by the SEIG increases when increasing the generator current as shown in Fig. 9(a). Due to change in torque, the voltage and frequency on the generator side tend to increase. The NSC absorbs the excess generated power and stores it in the BESS as can be seen from Fig. 9(d), which shows an increase in battery current. Due to this, the generator side

frequency is maintained constant as in Fig. 9(e). The NSC also effectively controls the power flow to the load side, keeping the load side voltage and current constant as shown in Fig. 9(b).

D. Performance Evaluation with Step Change in Illumination of PV

The effects of variation in solar illumination are shown in this subsection. To show the effects of solar illumination on the system, the following initial conditions are ensured.

- 1) the loads in the system remain constant;
- 2) turbine torque of the SEIG is considered to be constant at -85 Nm;
- 3) battery internal voltage is constant at 1800 V;
- 4) there are no other disturbances occurring in the generator or load side of the system.

Under the above conditions, the solar illumination varied in steps. The illumination is reduced from 1000 W/m² to 900 W/m² at 2.6 seconds, and again at 2.8 seconds, the illumination is increased from 1000 W/m² to 1200 W/m². The step variation in illumination is considered only to get a simple and clear view of its effects on the system.

As mentioned earlier, there are no disturbances or variations in both the generator and load sides of the system. Due to this, the generator and load side currents remain unaltered during the mentioned

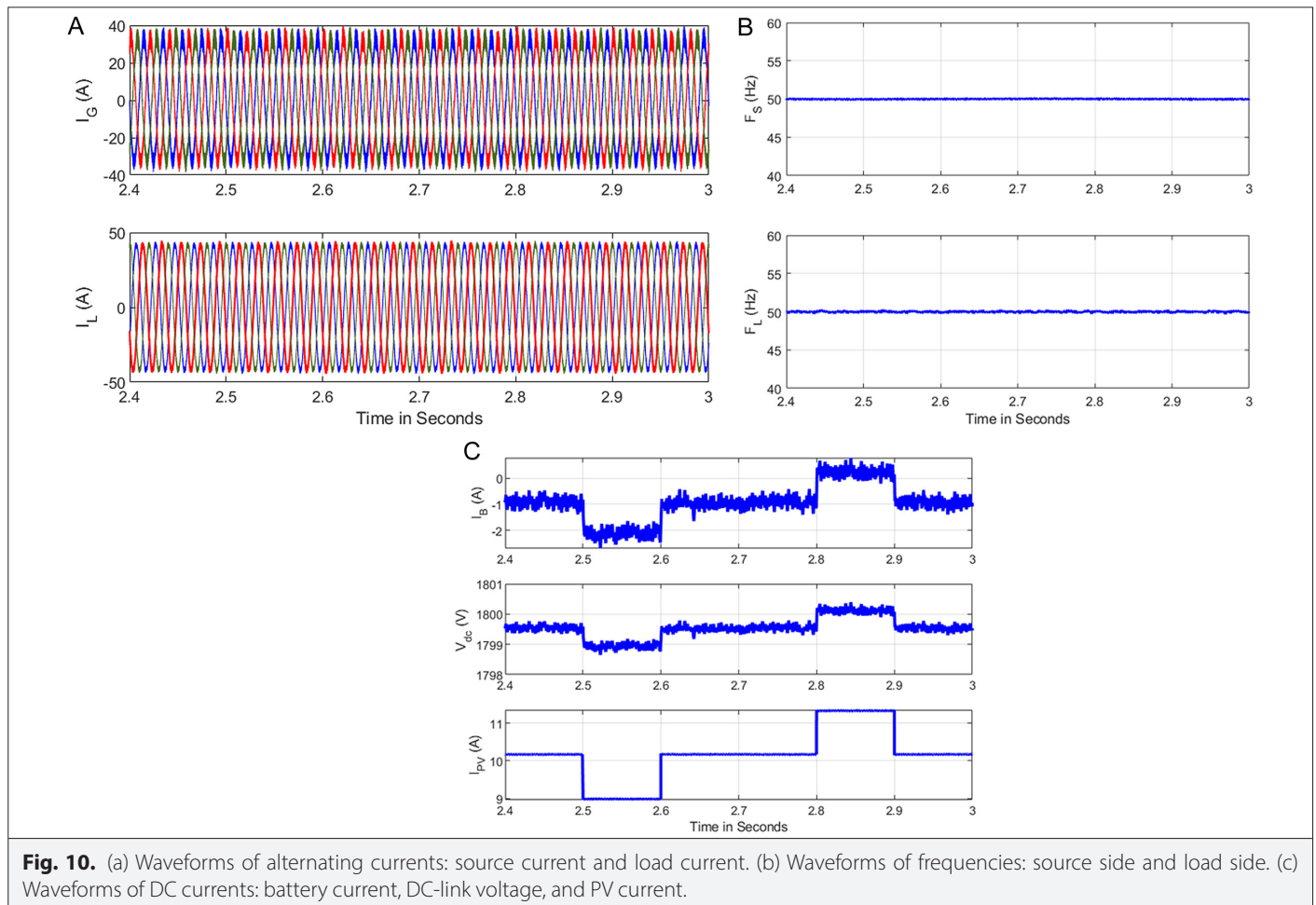


Fig. 10. (a) Waveforms of alternating currents: source current and load current. (b) Waveforms of frequencies: source side and load side. (c) Waveforms of DC currents: battery current, DC-link voltage, and PV current.

time interval of 2.6 seconds to 2.9 seconds, as can be seen from Fig. 10(a). The frequencies of both the generator and load sides, as in Fig. 10(b), also remain unchanged. Due to the variation in the solar radiation, only the DC side parameters are affected. As can be seen from Fig. 10(c) at 2.6 seconds, when the radiation reduces from 1000 W/m^2 to 900 W/m^2 , the current of the PV array " I_{pv} " reduces from 10.2 A to 9 A.

Before 2.6 seconds, the DC-link voltage was 1799.6 V which is less than the internal voltage of the battery. That causes a DC current of -1 A which is fed from the battery to the system. The negative sign of the battery current " I_b " means the current is fed in the system from the battery, that is the battery is discharging. Due to the reduction in radiation, the DC-link voltage reduces further to 1799V causing more battery current, that is -2.2A , which is fed into the system. It can be seen that the reduction in " I_{pv} " is managed by the increase in " I_b " so that the generator and load side voltages and frequencies remain constant. Similarly, during time 2.8–2.9 seconds, the solar radiation is increased from 1000 W/m^2 to 1200 W/m^2 , causing 11.2 A of " I_{pv} ". To manage the extra amount of " I_{pv} " the DC-link voltage increases from 1799.6 V to 1800.2 V, which is more than the internal voltage of the

battery. This reverses the current flow from -1 A to 0.2 A . The battery gets charged and stores the surplus amount of power that is being generated from the PV arrays.

C. Performance Evaluation with Source Disconnection

In this section, the NSC is tested for its capability of supplying continuous power to the load irrespective of partial and total disconnection of the sources. Here, a constant RL type load is considered at the load terminals. While supplying power to the load, at 2.3 seconds, the SEIG is taken out from the system which is clearly visible in Fig. 11(a). From 2.3 seconds to 2.5 seconds, the power is fed from the PV source and BESS. At 2.5 sec, the PV system is also disengaged from the system so the whole power required by the load is now directed from the BESS. Fig. 11(b) shows the contribution of the BESS during partial and total source disconnection.

As the discharging current builds, the DC-link voltage falls, this can be seen from Fig. 11(b). It very well may be seen that regardless of whether the SEIG and the PV are connected or disengaged, the NSC-based system is fit for providing continuous power to the load. The frequency and voltage of the hybrid system also remain fairly steady

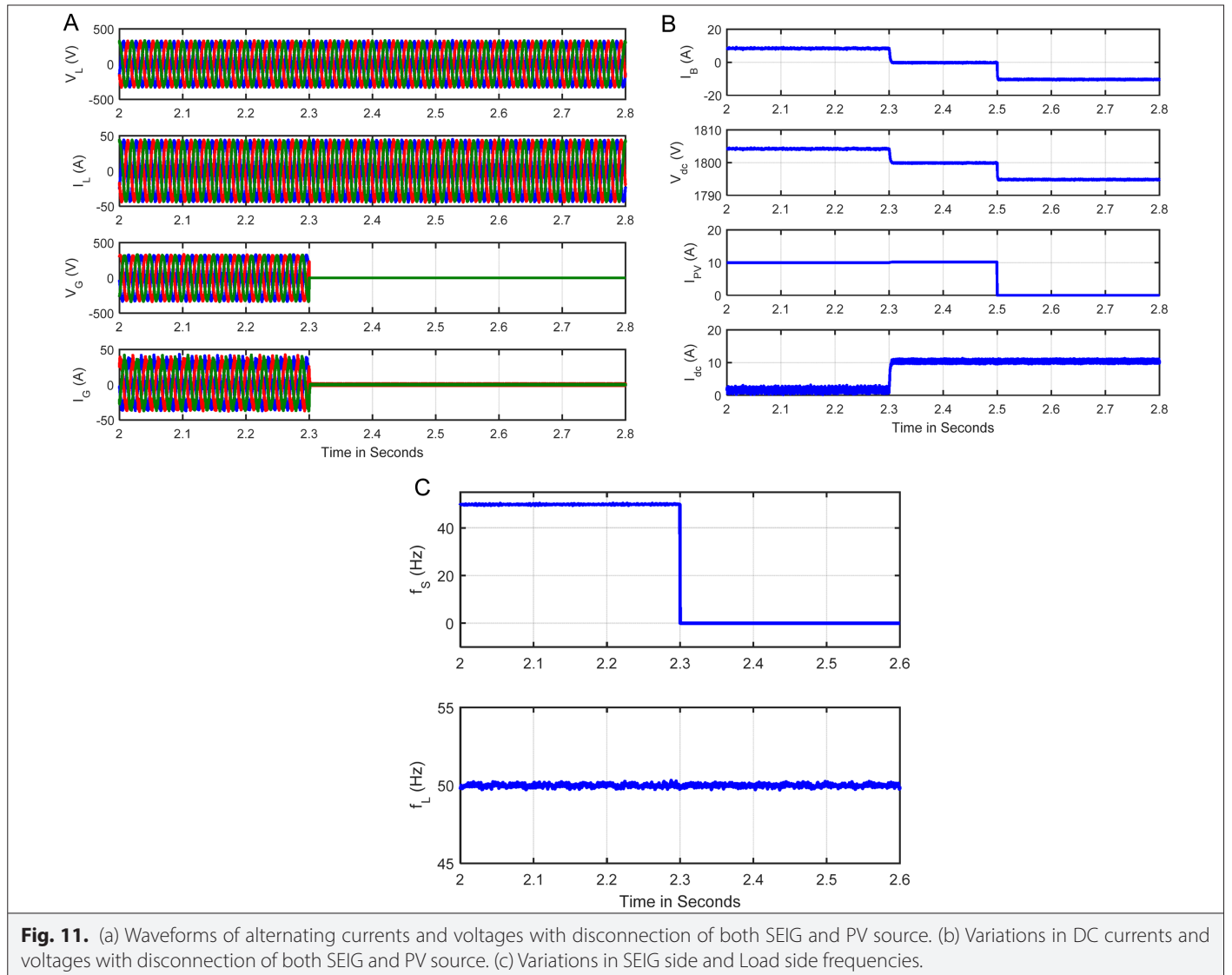


Fig. 11. (a) Waveforms of alternating currents and voltages with disconnection of both SEIG and PV source. (b) Variations in DC currents and voltages with disconnection of both SEIG and PV source. (c) Variations in SEIG side and Load side frequencies.

during the disconnection period which implies the robustness and efficacy of the load side control architecture. The frequency invariance of both source and load side is visible in Fig. 11(c).

V. CONCLUSIONS

In this study, most of the spotlight is focused on the control of voltage and frequency of the NSC-based hybrid system. The supply of continuous power to the load during different unsettling disturbances is another aspect of this study. The entire power control in this work is executed by the NSC which fills in as a proficient and powerful alternative of back to back converters for this purpose. The proposed system was found to be quite efficient and robust against various load disturbances and load switching, due to which the system frequencies and voltages are maintained at fairly constant values. Both the load and source side parameters remained fairly stable during various disturbances in the system. The BESS power was also efficiently managed by the control architecture and the NSC to provide continuous and uninterrupted power to the load. The control architecture was also fast enough to minimize the effects of the dynamic induction motor load switching. Hence, the NSC with its associated control structures can be considered to be efficient enough for integration and power control purpose in hybrid isolated systems. Apart from this, the future aspects, which could be investigated further, are the performance analysis with different robust and non-linear controllers, as well as the stability and sensitivity study of the proposed system.

Peer-review: Externally peer-reviewed.

Author Contributions: Concept – A.C., S.P.; Design – A.C., S.P.; Supervision – R.S., S.K.K.; Data Collection and/or Processing – S.P., A.C.; Analysis and/or Interpretation – S.P., A.C.; Literature Review – A.C.; Writing – A.C.; Critical Review – R.S., S.K.K.

Acknowledgment: The above-mentioned work has not been submitted to any other journal. No external funding has been drawn toward this research work. The first author has contributed toward designing, implementation, and writing of this technical article. The second author has given his efforts in finding out the problem formulation and design of the novel nine switch converter topology. The third and fourth authors have entirely supervised the work and discussed each and every point associated with it.

Declaration of Interests: The authors declare that they have no competing interest.

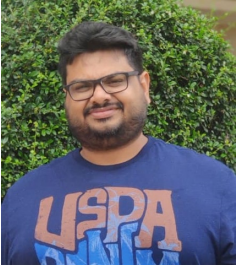
Funding: The authors declared that this study has received no financial support.

REFERENCES

1. T. F. Chan, "Capacitance requirements of self-excited induction generators," *IEEE Trans. Energy Convers.*, vol. 8, no. 2, pp. 304–311, 1993. [\[CrossRef\]](#)
2. Li Wang, and Jian-Yi Su, "Effects of long-shunt and short-shunt connections on voltage variations of a self-excited induction generator," *IEEE Trans. Energy Convers.*, vol. 12, no. 4, pp. 368–374, 1997. [\[CrossRef\]](#)
3. E. Bim, J. Szajner, and Y. Burian, "Voltage compensation of an induction generator with long-shunt connection," *IEEE Trans. Energy Convers.*, vol. 4, no. 3, pp. 526–530, 1989. [\[CrossRef\]](#)
4. S. M. Alghuwainem, "Steady-state analysis of an induction generator self-excited by a capacitor in parallel with a saturable reactor," *Electr. Mach. Power Syst.*, vol. 26, no. 6, pp. 617–625, 1998. [\[CrossRef\]](#)
5. M. A. Al-Saffar, E. C. Nho, and T. A. Lipo, "Controlled shunt capacitor self-excited induction generator," In Conference Record of 1998 IEEE Ind. Appl. Conference. Thirty-Third IAS Annual Meeting, Vol. 2. IEEE Publications, 1998 (Cat. No. 98CH36242).
6. B. Singh, L. Shridhar, and C. S. Jha, "Improvements in the performance of self-excited induction generator through series compensation," *IEE Proc. Gener. Transm. Distrib.*, vol. 146, no. 6, pp. 602–608, 1999. [\[CrossRef\]](#)
7. B. Singh, S. S. Murthy, and S. Gupta, "STATCOM-based voltage regulator for self-excited induction generator feeding nonlinear loads," *IEEE Trans. Ind. Electron.*, vol. 53, no. 5, pp. 1437–1452, 2006. [\[CrossRef\]](#)
8. B. Singh, S. S. Murthy, and S. Gupta, "Analysis and design of STATCOM-based voltage regulator for self-excited induction generators," *IEEE Trans. Energy Convers.*, vol. 19, no. 4, pp. 783–790, 2004. [\[CrossRef\]](#)
9. B. Singh, and L. B. Shilpakar, "Analysis of a novel solid state voltage regulator for a self-excited induction generator," *IEE Proc. Gener. Transm. Distrib.*, vol. 145, no. 6, pp. 647–655, 1998. [\[CrossRef\]](#)
10. B. Singh, S. S. Murthy, and S. Gupta, "Analysis and implementation of an electronic load controller for a self-excited induction generator," *IEE Proc. Gener. Transm. Distrib.*, vol. 151, no. 1, pp. 51–60, 2004. [\[CrossRef\]](#)
11. P. K. Goel, B. Singh, S. S. Murthy, and N. Kishore, "Isolated wind-hydro hybrid system using cage generators and battery storage," *IEEE Trans. Ind. Electron.*, vol. 58, no. 4, pp. 1141–1153, 2009. [\[CrossRef\]](#)
12. S. M. D. Dehnavi, M. Mohamadian, A. Yazdian, and F. Ashrafzadeh, "Space vectors modulation for nine-switch converters," *IEEE Trans. Power Electron.*, vol. 25, no. 6, pp. 1488–1496, 2009. [\[CrossRef\]](#)
13. W. Wang, A. Luo, X. Xu, L. Fang, T. M. Chau, and Z. Li, "Space vector pulse-width modulation algorithm and DC-side voltage control strategy of three-phase four-switch active power filters," *IET Power Electron.*, vol. 6, no. 1, pp. 125–135, 2013. [\[CrossRef\]](#)
14. G. He, Q. Chen, C. Kang, Q. Xia, and K. Poolla, "Cooperation of wind power and battery storage to provide frequency regulation in power markets," *IEEE Trans. Power Syst.*, vol. 32, no. 5, pp. 3559–3568, 2016. [\[CrossRef\]](#)
15. J. P. Barton, and D. G. Infield, "Energy storage and its use with intermittent renewable energy," *IEEE Trans. Energy Convers.*, vol. 19, no. 2, pp. 441–448, 2004. [\[CrossRef\]](#)
16. M. Quraan, T. Yeo, and P. Tricoli, "Design and control of modular multi-level converters for battery electric vehicles," *IEEE Trans. Power Electron.*, vol. 31, no. 1, pp. 507–517, 2015. [\[CrossRef\]](#)
17. S. Sikkabut *et al.*, "Control of high-energy high-power densities storage devices by Li-ion battery and supercapacitor for fuel cell/photovoltaic hybrid power plant for autonomous system applications," *IEEE Trans. Ind. Appl.*, vol. 52, no. 5, pp. 4395–4407, 2016. [\[CrossRef\]](#)
18. S. Mohanty, A. Choudhury, S. Pati, S. K. Kar, and P. Paritosh, "A SMC based nine Switch Converter Topology for Reliable and Efficient Control of Hybrid Autonomous System," In 9th Power India International Conference (PIICON). IEEE Publications, 2020, pp. 1–6.
19. A. Choudhury, S. Khatua, S. Pati, and S. K. Kar, "A reliable and efficient integration topology for autonomous hybrid systems using NSC," In International Conference on Electrical, Electronics and Computer Engineering (UPCON), Vol. 2019. IEEE Publications, 2019, pp. 1–6.
20. A. Choudhury, S. Mohanty, S. Pati, S. K. Kar, and R. K. Swain, "A Mamdani-FLC based nine Switch Converter Topology for Integration and Power Control of HAS," In International Conference on Computational Intelligence for Smart Power System and Sustainable Energy (CISPSSSE), Vol. 2020. IEEE Publications, 2020, pp. 1–6.



Abhijeet Choudhury completed his Bachelor of Technology from ITER, SOAU, Bhubaneswar. He completed his Masters of Technology in Power Electronics and Drives from the Department of Electrical Engineering, ITER, SOAU, Bhubaneswar. He is currently pursuing his PhD at Siksha O Anusandhan Deemed to be University in the Department of Electrical Engineering. He is currently working as a Faculty in the Department of Electrical Engineering at SOADU, Bhubaneswar. His research area includes AC/DC Microgrid, Electrical Machine & Drives, Integration and Power management of Hybrid autonomous system, Design of different converter topology, Renewable Energy, etc.



Dr. Swagat Pati completed his Bachelor of Technology from ITER, Bhubaneswar. He completed his Masters of Research in Power Electronics and Drives from NIT, Rourkela. He was awarded his PhD from Siksha O Anusandhan Deemed to be University. Presently he is working as an Assistant Professor in the Department of Electrical Engineering, ITER, Siksha O Anusandhan Deemed to be University. His research area includes Integration and Power control of Hybrid Renewable energy systems, design of new topology for power electronic converters, electric drives application, FACTS devices.



Dr. Sanjeeb Kumar Kar completed his Bachelor of Technology from the College of Engineering and Technology, Bhubaneswar. He completed his Masters of Technology and PhD from IIT, Kharagpur, from the Department of Electrical Engineering in Control Systems. Presently he is working as a Professor in the Department of Electrical Engineering, ITER, Siksha O Anusandhan Deemed to be University. His research area includes Control System, Power System Optimization, AGC, Integration and Power management. He has already guided more than a dozen of PhD in his career.



Renu Sharma is working as Professor and Head of Department in Department of Electrical Engineering in Siksha "O" Anusandhan Deemed to be University, Bhubaneswar, India. She is Senior Member IEEE, Life Member IE (India), Member IET, Life member ISTE, Life member ISSE, Past Chair WIE IEEE Bhubaneswar Sub Section. Her research areas are Smart Grid, Soft Computing, Solar Photovoltaic systems, Power System Scheduling, Evolutionary Algorithms, and Wireless Sensor Networks. She has published around 100 journal and conference articles of International Repute. She has organized several national and international conferences. She is guest editor of *Special Issue in International Journal of Power Electronics*, *Inderscience* and also, guest editor of *Special Issue in International Journal of Innovative Computing and Applications*, *Inderscience*. She has coordinated AICTE-sponsored FDP programs. She was one of the Plenary Chair PEDES 2020. She has around 21 years of leading impactful technical, professional, and educational experience. She was General Chair IEEE ODICON 2021, flagship conference IEEE WIECON-ECE 2020, Springer conference GTSCS-2020, IEPCC-2019, IEPCC 2021. She is serving publication Chair INDISCON-2022.